Journal of Power Sources 274 (2015) 229–236

Contents lists available at ScienceDirect

Journal of Power Sources

journal homepage: www.elsevier.com/locate/jpowsour

Highly stable multi-wall carbon nanotubes@poly(3,4-ethylenedioxythiophene)/poly(styrene sulfonate) core–shell composites with three-dimensional porous nano-network for electrochemical capacitors

Haihan Zhou [a, *], Gaoyi Han [a, *], Yunzhen Chang [a], Dongying Fu [b], Yaoming Xiao [a]

[a] Institute of Molecular Science, Key Laboratory of Chemical Biology and Molecular Engineering of Education Ministry, Shanxi University, Taiyuan 030006, China
[b] Institute of Crystalline Materials, Shanxi University, Taiyuan 030006, China

HIGHLIGHTS

- MWCNTs@PEDOT/PSS core–shell composites have been prepared.
- The composites show three-dimensional porous nanostructure.
- The effective composite of MWCNTs and PEDOT noticeably boosts the capacitive performance.
- The composites exhibit large capacitance and superb cycle stability.

GRAPHICAL ABSTRACT

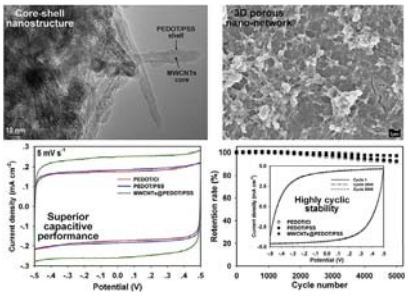

ARTICLE INFO

Article history:
Received 24 August 2014
Received in revised form
3 October 2014
Accepted 6 October 2014
Available online 15 October 2014

Keywords:
Supercapacitors
Carbon nanotubes
Core–shell
Nano-network
Cyclic stability

ABSTRACT

A facile and feasible electrochemical polymerization method has been used to construct the multi-wall carbon nanotubes@poly(3,4-ethylenedioxythiophene)/poly(styrene sulfonate) (MWCNTs@PEDOT/PSS) core–shell composites with three-dimensional (3D) porous nano-network microstructure. The composites are characterized with Fourier transform infrared spectroscopy, scanning electron microscope, and transmission electron microscopy. This special core–shell nanostructure can significantly reduce the ions diffusion distance and the 3D porous nano-network microstructure effectively enlarges the electrode/electrolyte interface. The electrochemical tests including cyclic voltammetry, galvanostatic charge/discharge measurements, and electrochemical impedance spectroscopy tests are performed, the results manifest the MWCNTs@PEDOT/PSS core–shell composites have superior capacitive behaviors and excellent cyclic stability, and a high areal capacitance of 98.1 mF cm^{-2} is achieved at 5 mV s^{-1} cyclic voltammetry scan. Furthermore, the MWCNTs@PEDOT/PSS composites exhibit obviously superior capacitive performance than that of PEDOT/PSS and PEDOT/Cl electrodes, indicating the effective composite of MWCNTs and PEDOT noticeably boosts the capacitive performance of PEDOT-based electrodes for electrochemical energy storage. Such a highly stable core–shell 3D network structural composite is very promising to be used as electrode materials for the high-performance electrochemical capacitors.

* Corresponding authors. Tel.: +86 351 7010699; fax: +86 351 7016358.
E-mail addresses: hhzhou@sxu.edu.cn (H. Zhou), han_gaoyis@sxu.edu.cn (G. Han).

http://dx.doi.org/10.1016/j.jpowsour.2014.10.044
0378-7753/

1. Introduction

The efficient use and storage of energy have attracted worldwide considerable research interest in recent years in response to the limited availability of fossil fuel and energy security concerns. As a type of high-efficiency devices of energy storage, a great deal of attention has been paid to electrochemical capacitors (also referred to as supercapacitors) due to their higher power density, cyclic stability than those of secondary batteries, whilst higher energy density than that of the dielectric capacitors [1–6].

Supercapacitors work on the basis of two charge-storage mechanisms: surface ion adsorption (electric double layer capacitance, EDLC) and redox reactions (pseudocapacitance) [7,8]. The electrodes of EDLC supercapacitors are usually made of different carbon materials, such as activated carbons, carbon nanotubes, carbon fibers and graphene, while the redox supercapacitors usually use transitional metal oxides and conducting polymers as the electrode materials [9–12]. Commonly, carbon materials show high power density and long cycle life but low capacitance, while transition metal oxides and conducting polymer have the large pseudocapacitance but exhibit some drawbacks like poor conductivity for transition metal oxides and low cycle life for conducting polymer [13,14]. For these reasons, considerable effort has been devoted to developing hybrid materials to obtain supercapacitor electrodes with superior performance [15–17].

Among all the carbon materials, carbon nanotubes (CNTs) have been widely investigated owing to their outstanding electric properties and nanoscale texture, such as high surface area, chemical stability, electrical conductivity and low cost [18–20]. In addition, conducting polymers possess the advantages of ease and versatility in synthesis, high inherent conductivity and low cost relative to the metal oxides [21], so combining the conducting polymer and CNTs seems to be a very attractive method, which has the potential to overcome the disadvantages of low energy density for CNTs and poor cycling performance for conducting polymers. The formation of nanocomposite materials through incorporating CNTs into polymer matrices is an interesting approach to enhance the properties of materials, because the resulting composites may exhibit characteristics that differ from those of the individual components. In the previous reports, conducting polymer/CNTs composites have been prepared with several approaches such as chemical polymerization, directly blending, grafting on CNTs, microwave-assisted method, and electrochemical polymerization [22–25]. Although these methods have been tried, the weak solubility and processibility of CNTs remain the hinder to achieve the high-performance electrode materials. Moreover, almost all the related researches focus on the mass specific capacitance of electrode materials, however, for applications such as small scale electronics and stationary energy storage devices where areal capacitance is a better indicator of the supercapacitor performance than mass specific capacitance [26,27]. Based on the consideration above, this study will improve the dispersity and solubility of CNTs through acid-treatment and adding PSS polyelectrolyte, and what's more, as the electrochemical polymerization show the advantages that the films can be deposited directly on the electrode substrates, and the film thickness can be easily controlled and the films are free from impurities (e.g. the oxidant and its reaction products) compared to chemical oxidative polymerization [28], we will use in situ electrochemical polymerization to prepare the high-performance conducting polymer/CNTs composite electrodes.

In this study, PEDOT was used because the PEDOT exhibits not only a high conductivity but also an unusual stability in the oxidized state compared to other types of conducting polymers (CPs) [29]. We depicted a simple strategy to synthesize the MWCNTs@PEDOT/PSS composites by a facile electrochemical codeposition method. Thereinto, MWCNTs was acid-treated to promote the dispersity and also acted as the counter-ions, PSS polyelectrolyte was added to system serving as supporting electrolyte to promote the conductivity of solution, also improve the solubility of CNTs and as the counter-ions. As the comparison, PEDOT/PSS and PEDOT/Cl electrodes have also been prepared under the polymerization system with the same electrochemical procedure. The compositions and morphology as well as the microstructures of the composites were studied with Fourier transform infrared spectroscopy (FT-IR), scanning electron microscope (SEM), and transmission electron microscopy (TEM). Their electrochemical behaviors were compared using cyclic voltammetry (CV), galvanostatic charge/discharge (GCD) measurements, and electrochemical impedance spectroscopy (EIS). The composites of PEDOT and MWCNTs obtained by the feasible and effective electrochemical method are expected to possess a special microstructure and can significantly improve the performances of the pristine PEDOT electrodes, consequently achieve the higher energy density, power capability and cycle stability.

2. Experimental

2.1. Materials

3,4-ethylenedioxythiophene (EDOT, Ourchem®, 99%) was purchased from Sinopharm Chemical Reagent Co. Ltd (Shanghai, China), MWCNTs were purchased from Chengdu Organic Chemicals Co. Ltd (Chengdu, China), the length of the MWCNTs was 0.5–2 μm. Poly(styrene sulfonic acid) sodium salt (PSS, M.W. = 70,000) was purchased from Alfa Aesar (Ward Hill, US). FTO conducting glasses were obtained from Dalian Heptachroma SolarTech (DHS-FTO22-8-02, 8 Ω $\square^{-1}$), 1 cm × 1 cm conductive areas were exposed as the substrate for electrochemical deposition. Prior to use, the glasses were ultrasonically cleaned with acetone and deionized water successively.

2.2. Electrode preparation

The MWCNTs@PEDOT/PSS composite films were synthesized electrochemically via in situ polymerization/codeposition from an aqueous solution containing acid-treated MWCNTs, PSS, and EDOT monomer, and the process of acid treatment of MWCNTs and codeposition were as follows:

Firstly, MWCNTs were pretreated in 3 M HNO_3 at 140 °C under magnetic stirring for at least 72 h to remove the metal catalysts. Then the pretreated MWCNTs were shortened and functionalized with carboxyl group (−COOH) by ultrasonicating in a mixture of concentrated H_2SO_4 and HNO_3 (v: v = 3:1) at 40 °C for 2 h, followed by thorough rinsing with deionized water until the pH reached about 6.0. Finally, the carboxylated MWCNTs (MWCNTs−COOH) were collected and dried at 60 °C for 48 h.

For the procedure of electrochemical codeposition, an aqueous solution containing 2 mg mL^{-1} MWCNTs−COOH, and 0.01 M PSS polyelectrolyte was dispersed under ultrasonication for about 15 min to form a metastable homogenous colloidal solution, in which PSS serves as supporting electrolyte as well as counter-ions, after that, 0.01 M EDOT monomer was added into the polymerized solution with ultrasonic dispersion. Subsequently, MWCNTs@PEDOT/PSS composite films were electrodeposited onto the FTO conducting glass with a galvanostatic mode, in which a current of 1.0 mA cm^{-2} was applied for 30 min. After that, the composite films-deposited glasses were washed with adequate deionized water to remove the unreacted substance, followed by drying at room temperature under ambient air environment, which is shown in Fig. 1a (left). During the deposition, the cleaned FTO conducting

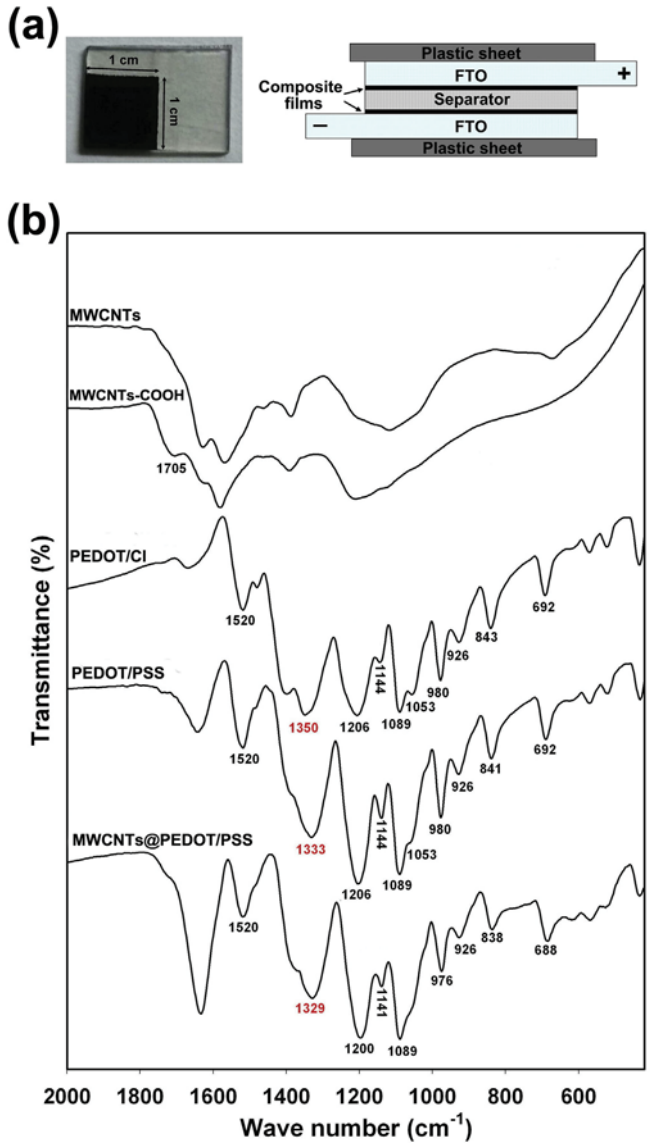

Fig. 1. (a) The digital photo of MWCNTs@PEDOT/PSS films-deposited FTO conducting glass (left) and the supercapacitor cells consisted of two pieces of symmetric composite films-deposited FTO conducting glass for electrochemical measurements (right); (b) FT-IR spectra of MWCNTs, MWCNTs–COOH, PEDOT/Cl, PEDOT/PSS, and MWCNTs@PEDOT/PSS composites.

glass was fixed in a two-electrode cell with a large-area Pt sheet acting as the counter electrode and pseudo-reference electrode. In order to compare MWCNTs@PEDOT/PSS composite films with pristine PEDOT films, PEDOT/PSS and PEDOT/Cl films were electrodeposited under the same procedure from an aqueous solution of 0.01 M EDOT mixed with 0.1 M PSS and 0.1 M KCl, respectively.

2.3. Composition and morphology characterization

FT-IR spectra of as-received MWCNTs, MWCNTs–COOH, PEDOT/Cl, PEDOT/PSS, and MWCNTs@PEDOT/PSS were obtained with a Bruker Tensor 27 FT-IR spectrometer. PEDOT/Cl, PEDOT/PSS, and MWCNTs@PEDOT/PSS films were scraped from the surface of films-deposited onto ITO conducting glasses, all test samples were prepared by potassium bromide tabletting. The surface morphology of the PEDOT/Cl, PEDOT/PSS, and MWCNTs@PEDOT/PSS composite films was observed using a field emission scanning electron microscope (JSM-6701F, JEOL) operated with a voltage of 10.0 kV. The microstructures of MWCNT–COOH and MWCNTs@PEDOT/PSS composites were examined with a high-resolution transmission electron microscopy (JEM-2100, JEOL) operated at 200 kV.

2.4. Electrochemical measurements

For the electrochemical measurements, the capacitor cells (Fig. 1a, right) were assembled with two pieces of composite films-deposited FTO conducting glasses (one oxidized and one reduced) as the two electrodes, a filter paper soaked with 1.0 M KCl electrolyte served as the separator, the conducting glass itself was used as the current collector. All the electrochemical measurements were carried out on an electrochemical workstation (CHI 660B, Chenhua, China) using two-electrode system. The CV measurements were performed between potentials of −0.5 to 0.5 V, and the scan rates ranged from 5 to 200 mV s^{-1}. The GCD tests were performed at varying current density with the cutoff voltage of −0.5 and 0.5 V. The EIS were measured using 5 mV (rms) AC sinusoid signal and at a frequency range from 100 K to 0.01 Hz at the open circuit potential. During the aforementioned electrochemical tests, the assembled cells were wrapped with a preservative film to prevent the volatilization of electrolyte.

3. Results and discussion

3.1. FT-IR spectroscopy

In the experimental design, carboxylic group was covalently attached to MWCNTs with the acid treatment, and the carboxylic MWCNTs worked as a dopant during the polymerization of PEDOT. The FT-IR spectroscopy of as-received MWCNTs, MWCNTs–COOH, PEDOT/Cl, PEDOT/PSS, and MWCNTs@PEDOT/PSS are presented in Fig. 1b. Compared with the spectra of the pure MWCNT, the appearance of C=O stretching vibration peak of the carboxylic group at 1705 cm^{-1} confirms the carboxylic functionalization of the MWCNTs in the MWCNTs–COOH spectrum [30]. For the PEDOT/Cl spectrum, the vibrations around 1350 and 1520 cm^{-1} originate from the quinoid structure and stretching modes of C–C and C=C in the thiophene ring, respectively [31]. Vibrations at 1206, 1144, 1089, and 1053 cm^{-1} are attributed to stretching of the C–O–C bond in the ethylenedioxy group, peak at 926 cm^{-1} is ascribed to the ethylenedioxy ring deformation mode, and the vibration modes of the C–S bond in the thiophene ring are observed at 692, 843 and 980 cm^{-1} [32–34]. With the PEDOT/Cl spectrum as the reference, the spectra of both PEDOT/PSS and MWCNTs@PEDOT/PSS show the characteristic peaks of PEDOT. The only difference is that the vibration band attributed to C–C stretching in the thiophene ring in PEDOT/PSS and MWCNTs@PEDOT/PSS has a redshift from 1350 to 1333 and 1329 cm^{-1} (marked with red). This is related to the electrostatic interaction between the PEDOT cations and the PSS anions as well as the inclusion of MWCNTs–COOH in the polymer films. It should be noted that MWCNTs–COOH bands are scarcely detectable in the MWCNTs@PEDOT/PSS spectrum, probably because either they are too weak or overlapped with the absorption peak of PEDOT. In summary, the formation of MWCNTs@PEDOT/PSS composite films was confirmed by the study of FT-IR spectra.

3.2. Morphology

It is well known that electrochemical performance of an electrode is strongly influenced by its microstructure and the active surface area accessible to the electrolytic ions [35]. The SEM images of the PEDOT/Cl, PEDOT/PSS, and MWCNTs@PEDOT/PSS electrodes prepared are displayed in Fig. 2. For PEDOT/Cl films (Fig. 2a and b),

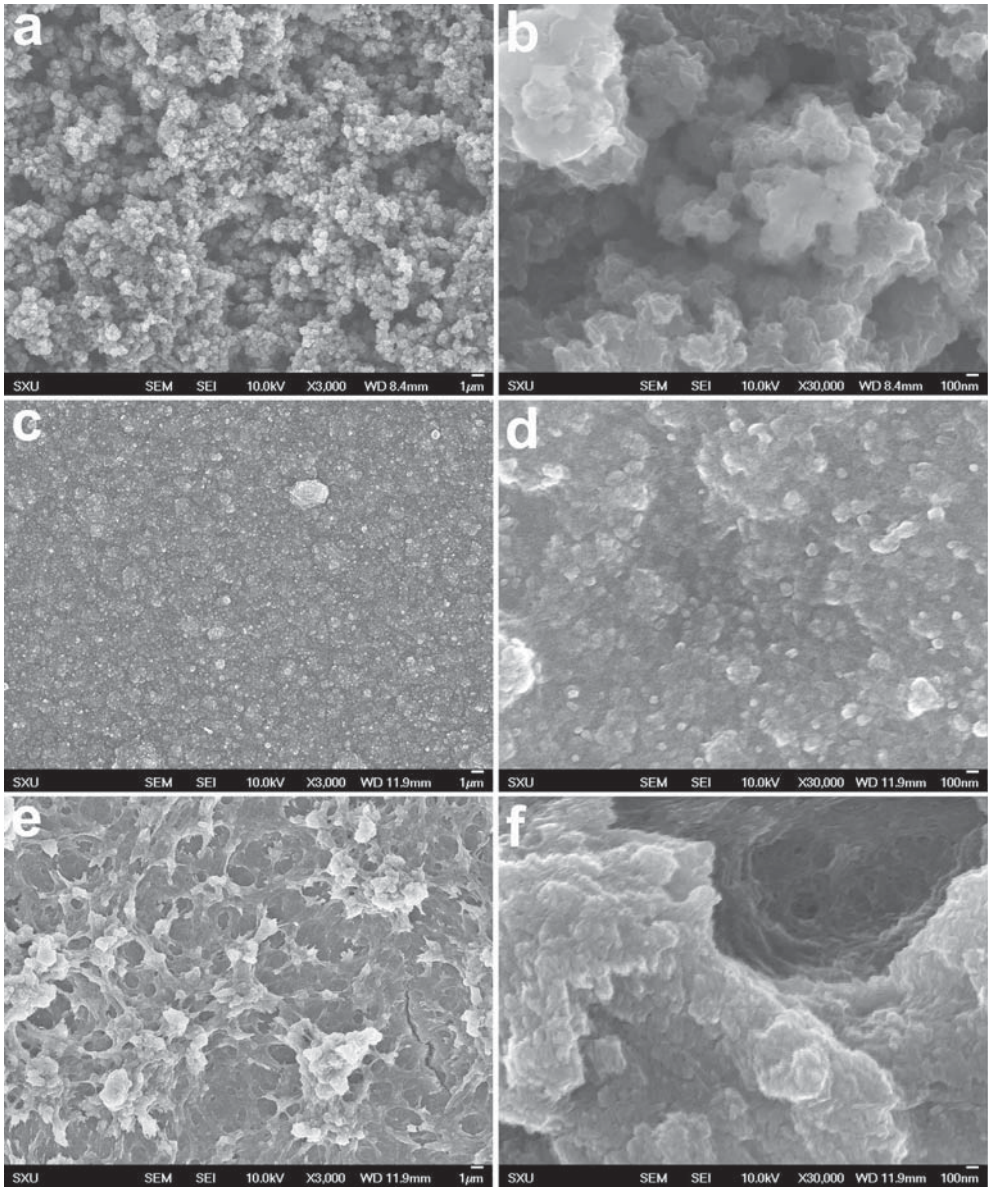

Fig. 2. SEM images of PEDOT/Cl (a, b), PEDOT/PSS (c, d) and MWCNTs@PEDOT/PSS (e, f) films with low (a, c, e) and high (b, d, f) magnification.

cumulate grains with an average diameter of ~200 nm and aggregated deposits are observed, and the films show the feature of porosity, which would be beneficial to the access of electrolyte. Fig. 2c and d exhibits the SEM images of PEDOT/PSS films, presenting a dense and compact microstructure, and the PEDOT/PSS films essentially comprise of clusters formed by piling up of smaller grains to yield larger particles of various size. In contrast to those two types of films, the MWCNTs@PEDOT/PSS composite films (Fig. 2e) exhibit a very different morphology that a three-dimensional porous microstructure composed of some nodes, furthermore, the SEM image of MWCNTs@PEDOT/PSS films at high magnification (Fig. 2f) depicts a very rough surface where the PEDOT and PEDOT/PSS polymer have encased bundles of MWCNTs, with a highly large porous structure apparent. This microstructure of 3D porous nano-network is very desirable because it maximizes the electrochemical surface area, potentially allowing large capacitances to be obtained. Furthermore, the SEM characterization suggests that MWCNTs possibly act as an electron conducting network for the composite film, thus enhancing the electron conductivity and improving the mechanical performance. Moreover, the porous surface would significantly enlarge the electrode/electrolyte interface and facilitate ion transfer within the bulk films, leading to the advanced electrochemical performance over PPy/Cl and PPy/PSS films, and this will be testified in the following section of electrochemical tests.

In order to further observe the composite morphology of MWCNTs@PEDOT/PSS films, TEM characterization was made and the images are shown in Fig. 3. Fig. 3a shows the morphology of MWCNTs–COOH, we can see that the MWCNTs–COOH are very long and entangled with each other as a spider web, indicating the MWCNTs–COOH show the well dispersibility after acid-treatment. Fig. 3b exhibits the TEM image of MWCNTs–COOH at high magnification, it can be observed that MWCNTs–COOH show a hollow structure with an outer diameter of ~10 nm, and the central canal of MWCNTs allows for easy accessibility of ions to the electrode/electrolyte interface. Like the SEM characterization, as shown in Fig. 3c, the morphology of MWCNTs@PEDOT/PSS composite films depict a very rough surface where the PEDOT and PEDOT/PSS

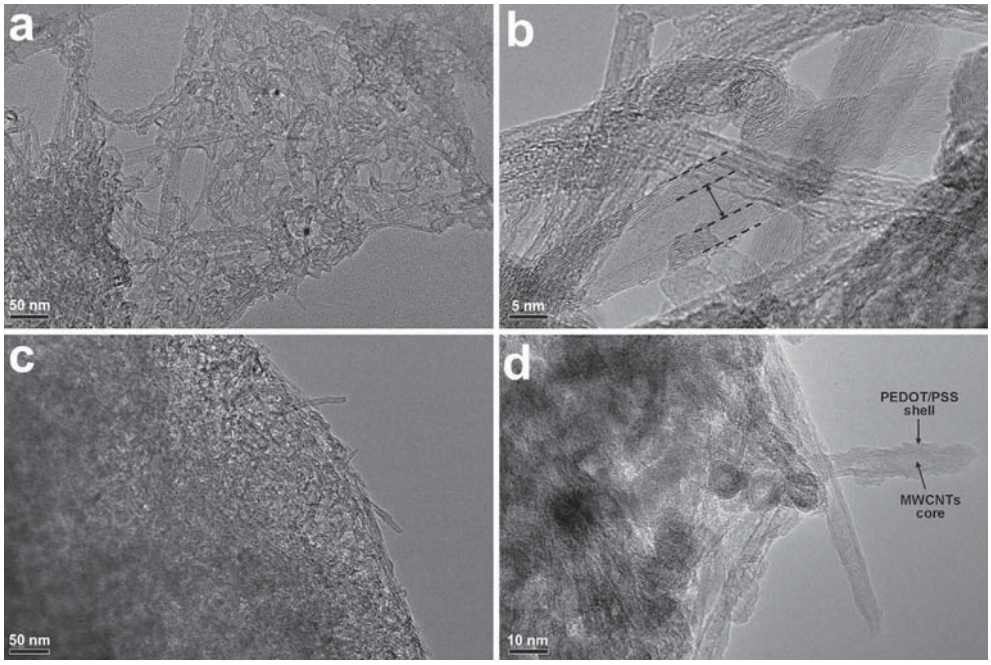

Fig. 3. TEM images of the MWCNTs–COOH (a, b) and MWCNTs@PEDOT/PSS composites (c, d) taken at low (a, c) and high (b, d) magnification.

polymer have encased bundles of MWCNTs, and the TEM image of composites at high magnification (Fig. 3d) displays the MWCNTs are coated with the PEDOT/PSS polymer (arrow indicated). Herein, the MWCNTs and the PEDOT coated forms the core–shell nanostructure, which can significantly reduce the ions diffusion distance and improve the charge transfer of pure PEDOT as a result of the high conductivity of MWCNTs. On the whole, the morphology characterization reveals that the micro- and nano-meter pores in the MWCNTs@PEDOT/PSS composites which can provide enough pathways for the movement of ions and solvent molecules within the composite films. The tangled MWCNTs rods incorporated into composite films probably act as a conductive network and the formed core–shell microstructure can improve the electrochemical properties as discussed below.

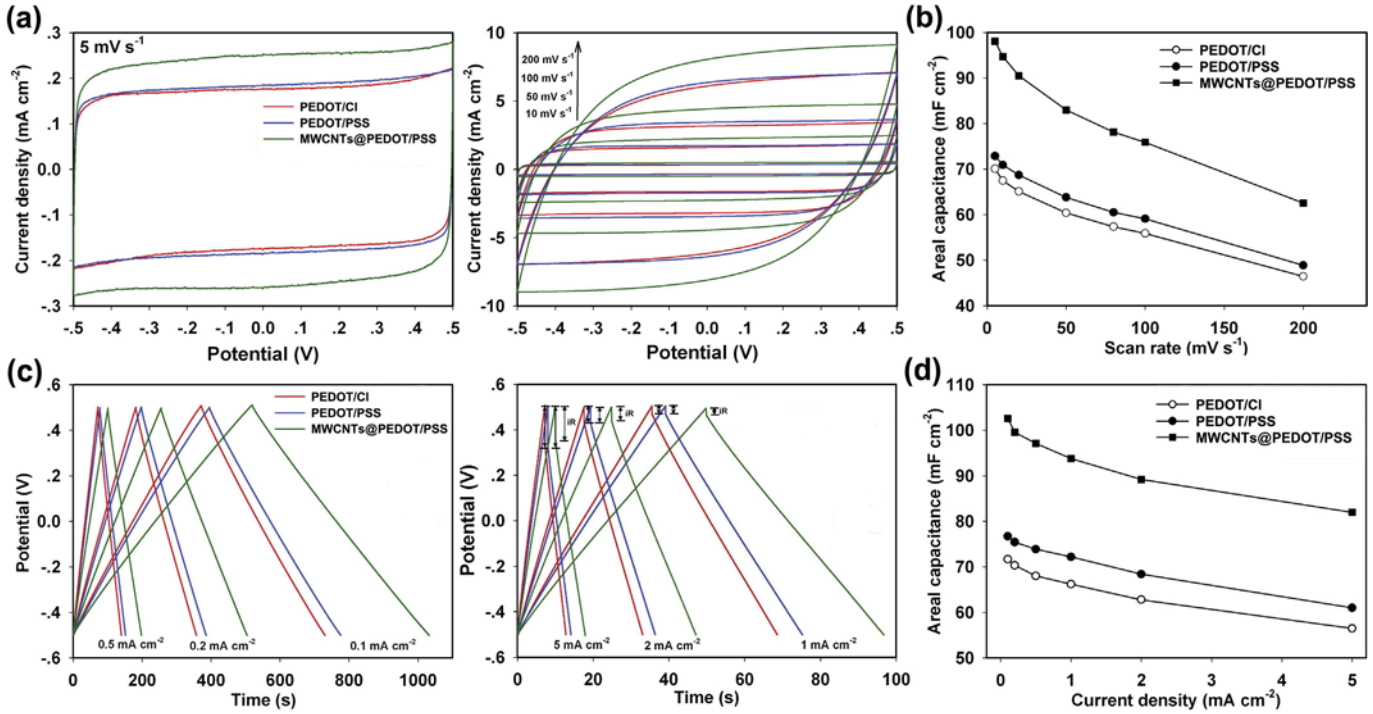

Fig. 4. (a) CV curves of the supercapacitor cells assembled by PEDOT/Cl, PEDOT/PSS and MWCNTs@PEDOT/PSS composites electrodes at different scan rates range from 5 mV s^{-1} to 200 mV s^{-1}; (b) relationship of the areal capacitance with CV scan rate for PEDOT/Cl, PEDOT/PSS and MWCNTs@PEDOT/PSS composites electrodes; (c) GCD curves of the supercapacitor cells assembled by PEDOT/Cl, PEDOT/PSS and MWCNTs@PEDOT/PSS composites electrodes at different GCD current densities; (d) areal capacitance *vs.* GCD current density for PEDOT/Cl, PEDOT/PSS and MWCNTs@PEDOT/PSS composites electrodes.

3.3. Electrochemical properties

In this study, the electrochemical behavior was investigated with two-electrode system, allowing a good estimation of materials performance in electrochemical capacitors [36]. CV was employed to evaluate the capacitive performance of PEDOT/Cl, PEDOT/PSS, and MWCNTs@PEDOT/PSS composite electrodes, and the resulting CV at varying scan rates rang from 5 to 200 mV s^{-1} is show in Fig. 4a. Commonly, the capacitor assembled by two pieces of identical electrodes are tested by two-electrode system, one piece of composite is oxidized and the other is reduced during the test, which will make the oxidation/reduction peaks of PEDOT unobvious and show the rectangular CV shape. It can be observed from the 5 mV s^{-1} plots that the MWCNTs@PEDOT/PSS electrodes show more rectangular-like shape and larger areal CV curve compared with those of the PEDOT/PSS and PEDOT/Cl electrodes, indicating the MWCNTs@PEDOT/PSS electrodes exhibit more ideal capacitive behavior as a result of the incorporation of MWCNTs into the PEDOT matrix. Furthermore, the rectangular-like CV curves with the almost symmetric *I*–*E* responses can be also observed at higher scan rates range from 10 to 200 mV s^{-1} and the current obviously increased with increasing scan rate, demonstrating that the MWCNTs@PEDOT/PSS electrodes have good rate capability, and the MWCNTs@PEDOT/PSS electrodes still show the larger areal CV curves than those of the PEDOT/PSS and PEDOT/Cl electrodes at all scan rates. Aiming for the applications such as small scale electronics and stationary energy storage devices, areal capacitance is a better indicator of the supercapacitor performance than mass specific capacitance [37,38], so this research focuses on the areal capacitance of electrodes. On the basis of the CV curves, the areal capacitance (C_S) value of a single electrode can be calculated according to the following Equation (1):

$$C_S = \left(\int i\mathrm{d}V\right)/(S \times \Delta V \times \nu) \quad (1)$$

where C_S is the areal capacitance in F cm^{-2}, $\int i$dV the integrated area of the CV curve, *S* the surface area of active materials in the single electrode in cm^2 and it is fixed at 1 cm^2 in this study, ΔV the scanning potential window in V and ν the scan rate in V s^{-1}.

Fig. 4b shows the plots of the areal capacitance *vs.* CV scan rates for the three types of electrodes, the PEDOT/Cl electrodes display the areal capacitance of 70.1 mF cm^{-2} at 5 mV s^{-1} while 72.9 mF cm^{-2} at 5 mV s^{-1} for PEDOT/PSS electrodes, however, when the MWCNTs are incorporated into the PEDOT matrix, the areal capacitance sharply increase to 98.1 mF cm^{-2} at 5 mV s^{-1} (increase of ~26%) and 94.7 mF cm^{-2} at 10 mV s^{-1} for the MWCNTs@PEDOT/PSS electrodes, and it is also higher than that of PANI/graphite oxide composites (25 mF cm^{-2} at 5 mV s^{-1}) and TiO_2@PPy core–shell nanowires electrode (64.6 mF cm^{-2} at 10 mV s^{-1}) reported previously [38,39]. Furthermore, the MWCNTs@PEDOT/PSS electrodes have a consistent higher areal capacitance value at all other scan rates compared to the PEDOT/PSS and PEDOT/Cl electrodes. The CV results indicate the incorporation of MWCNTs into the composites remarkably boost the capacitive performance for PEDOT-based supercapacitors.

Fig. 4c depicts the GCD curves of PEDOT/Cl, PEDOT/PSS, and MWCNTs@PEDOT/PSS electrodes at the varying current density rang from 0.1 to 5 mA cm^{-2}. It can be seen from the 0.1 mA cm^{-2} plots that the three types of electrodes exhibit triangular-shape charge/discharge curves, but the MWCNTs@PEDOT/PSS electrodes have the longest discharge time. The columbic efficiency (η) can be determined by calculating the ratio of discharge time t_d to charge time t_c according to the GCD curves. At the current density of 0.1 mA cm^{-2}, the η of MWCNTs@PEDOT/PSS electrodes is 98.9%, which is higher than 96.3% of PEDOT/PSS and 96.2% for PEDOT/Cl electrodes. Moreover, as exhibited in Fig. 4c, the GCD curves at higher current density range from 1 to 5 mA cm^{-2} also show the same results that MWCNTs@PEDOT/PSS electrodes have the longest discharge time. Meanwhile, the MWCNTs@PEDOT/PSS electrodes also show the lower *i*R drops at all GCD current densities. It should be pointed out that *i*R drop is usually caused by the overall internal resistance of the devices [37], indicating the capacitor cells assembled with MWCNTs@PEDOT/PSS electrodes have the lower internal resistance. The low internal resistance is important for energy storage devices, because it will facilitate decreasing the produce of unwanted heat during the processes of charging/discharging [40]. Based on the GCD curves measured by chronopotentiometry, the areal capacitance (C_S) value of a single electrode can be evaluated using the following Equation (2):

$$C_S = (2 \times i \times t)/(S \times \Delta V) \quad (2)$$

where C_S is the areal capacitance in F cm^{-2}, *i* the discharge current in A, *t* the discharge time in s, *S* the surface area of the active materials on the single electrode in cm^2 and ΔV the scan potential window in V.

Fig. 4d compares the areal capacitance value of the three types of electrodes, the MWCNTs@PEDOT/PSS electrodes display the areal capacitance of 102.6 mF cm^{-2} at 0.1 mA cm^{-2}, which is higher than those of PEDOT/PSS (76.7 mF cm^{-2} at 0.1 mA cm^{-2}) and PEDOT/Cl electrodes (71.7 mF cm^{-2} at 0.1 mA cm^{-2}), and the MWCNTs@PEDOT/PSS electrodes show the largest areal capacitance value at all varying GCD current densities, which is consistent with the CV results. Likewise, the GCD tests also indicate the incorporation of MWCNTs into the composites noticeably improve the capacitive performance of electrodes. The significant improvement of capacitance for the composites can be derived from the pronounced increase of specific surface area as the incorporation of MWCNTs, in addition, combining the morphology characterization, the formed nanostructure of 3D porous network and the core–shell nanostructure of PEDOT/PSS-coated MWCNTs can significantly reduce the ions diffusion distance and adequately take advantage of the double layer capacitance from MWCNTs and Faradaic pseudocapacitance from PEDOT.

In order to further comparing the electrochemical performance of the three types of electrodes applied for electrochemical capacitor, the EIS tests were carried out and the obtained Nyquist plots at open-circuit potentials are illustrated in Fig. 5a. It can be seen that the three types of electrodes show a vertical trend at low frequencies region, indicating the capacitive behavior according to the equivalent circuit theory [41], no or negligible semicircle observed at high frequency region for the three types of electrodes is ascribed to the low interfacial charge-transfer resistance as their high conductivity of films [31]. The equivalent series resistance (ESR) can be obtained from the intersection of the curve at the *x*-axis, it mainly arises from the electrolyte, the intrinsic resistance of the active material, and the contact resistance at the active material/current collector interface [38]. We can observe from the inset of Fig. 5a that the intercept at *x*-axis for the impedance plot of MWCNTs@PEDOT/PSS electrodes is the smallest, manifesting the lowest ESR of the assembled capacitor with MWCNTs@PEDOT/PSS electrodes. Knee frequency (f_{knee}) is another important information that can be obtained from the plots at higher frequencies, it is the maximum frequency at which predominant capacitive behavior can be maintained, beyond which the capacitive behavior is replaced by the more inclined diffusion line. The f_{knee} is determined by the crossing of Warburg-type line (inclined 45°) and low-frequency vertical line, the higher knee frequency means the lower diffusion impedance and faster charge transfer rates [42]. We

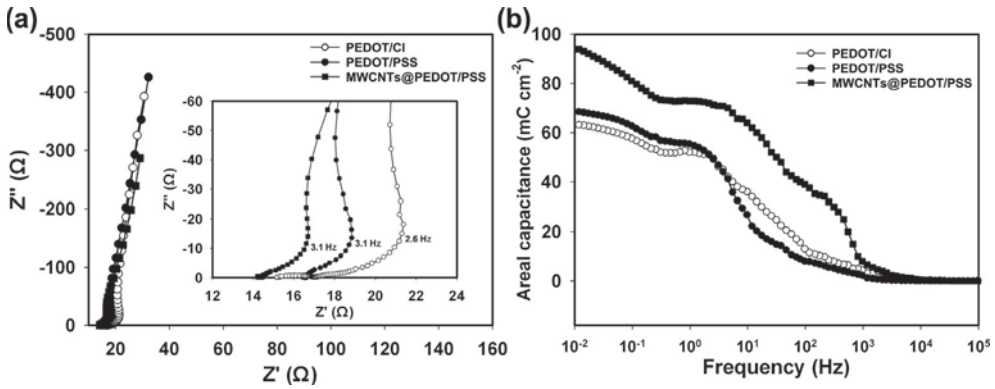

Fig. 5. (a) Nyquist plots of the supercapacitor cells assembled by PEDOT/Cl, PEDOT/PSS and MWCNTs@PEDOT/PSS composites electrodes, insert is the EIS in high-frequency region; (b) The relationship of conversion areal capacitance with frequency for PEDOT/Cl, PEDOT/PSS and MWCNTs@PEDOT/PSS composites electrodes.

can see from the inset of Fig. 5a that MWCNTs@PEDOT/PSS electrodes display the highest f_{knee}, this will facilitate the rapid charge/discharge performance, as the results exhibited in the CV and GCD tests. Fig. 5b presents the conversion capacitance obtained from EIS. The areal capacitance values of single electrode can be calculated from the following Equation (3) [41]:

$$C_S = -1 \Big/ \left(\pi S f Z''\right) \tag{3}$$

Thereinto, C_S is the areal capacitance in F cm^{-2}, f the frequency in Hz, Z'' the imaginary part of EIS in Ω, and S the geometric surface area of active materials on single electrode (1 cm^2 in this study). It can be seen from Fig. 5b that MWCNTs@PEDOT/PSS electrodes exhibit the highest areal capacitance at the whole frequency region compared with those of PEDOT/PSS and PEDOT/Cl electrodes, which is in good agreement with the results measured in CV and GCD tests. The EIS tests further confirm the superiority of MWCNTs@PEDOT/PSS composites used for electrochemical capacitors.

3.4. Ragone plot and cyclic stability

The areal energy and power density are usually used for evaluating thin film micro-batteries because the comparison has no dependence on the choice of other components including substrates and protective packaging [43]. The areal energy density and power density of the single electrode depicted in the Ragone plot can be calculated by using the Equations (4) and (5), respectively [38].

$$E = \frac{\frac{1}{2} C_S \Delta V^2}{3600} \tag{4}$$

$$P = \frac{3600E}{t} \tag{5}$$

where E is the areal energy density in Wh cm^{-2}, P the areal power density in W cm^{-2}, C_S the areal capacitance in F cm^{-2}, ΔV the potential window (excluding iR drop in the beginning of the discharge) in V and t the discharge time in s.

Fig. 6 shows the corresponding Ragone plots based on the area of the films according to the above formulas. Obviously, the MWCNTs@PEDOT/PSS electrodes present the higher energy and power densities than those of PEDOT/PSS and PEDOT/Cl electrodes all the time. The MWCNTs@PEDOT/PSS electrodes deliver an energy density of 14.2 μWh cm^{-2} at a power density of 99.7 μW cm^{-2}, while it maintains 9.69 μWh cm^{-2} at 4256 μW cm^{-2}, presenting higher energy density and power density compared with previous reports on conducting polymers [38]. This high power capability is an indication of fast kinetic reaction in the MWCNTs@PEDOT/PSS composites, which can be attributed to the high electronic conductivity of the CNT network and porous core–shell microstructures of composites permitting counter-ions which could diffuse into the polymer and provide a short diffusion distance to facilitate the ion transport.

In this study, 5000 CV cycles at the scan rate of 100 mV s^{-1} were carried out to investigate the cycle stability of the MWCNTs@PEDOT/PSS electrodes and the result is shown in Fig. 7. We can observe that the cycle measurements for MWCNTs@PEDOT/PSS electrodes cause an increase in the capacitance up to 1000 cycles. It can be possibly related to a cycling measurement induced improvement in the surface wetting of the electrode [44,45], which is attributed to the large electrochemical surface area caused by the incorporated MWCNTs, leading to more available electroactive surface area with the cycles. Especially, the MWCNTs@PEDOT/PSS composites retain 97.8% of the initial capacitance after 5000 cycles, highlighting the MWCNTs@PEDOT/PSS electrodes have the excellent electrochemical stability, as the comparison, the capacitive retention rate of PEDOT/PSS and PEDOT/Cl electrodes decreases to 92.6% and 91.7%, respectively. The excellent stability of composites can be attributed to the incorporated MWCNTs enhances the mechanical strength of the composites and prevents the CPs from swelling and shrinking during the long-term cycles. Generally, the significant improvement in the capacitive behavior and excellent stability for MWCNTs@PEDOT/PSS core–shell composites may be attributed to the following reasons: firstly, the incorporation of

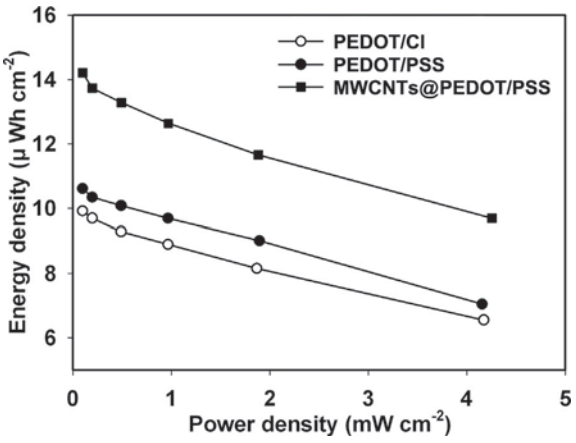

Fig. 6. Ragone plots of PEDOT/Cl, PEDOT/PSS and MWCNTs@PEDOT/PSS composites electrodes.

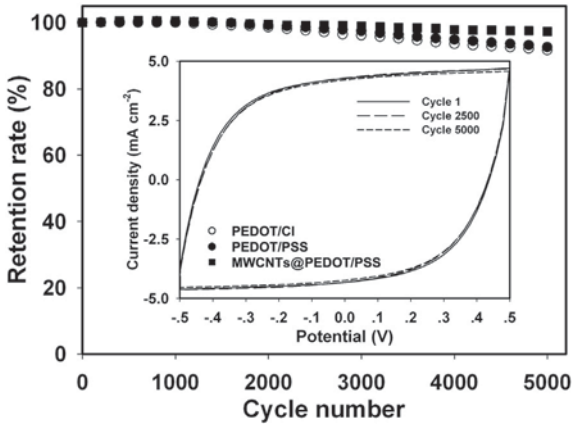

Fig. 7. The relationship of capacitance retention rate and cycle number for PEDOT/Cl, PEDOT/PSS and MWCNTs@PEDOT/PSS composites at 100 mV s^{-1} CV scan for 5000 cycles. The inset is the CV curves of the supercapacitor cells assembled by MWCNTs@PEDOT/PSS electrodes at different scan cycles.

large anions MWCNTs makes the polymer films less compact and form the nanostructure of 3D porous network with large specific surface area; Secondly, the formed core–shell nanostructure with MWCNTs core and PEDOT/PSS shell, which may be beneficial to enhance the rates and accessibility of ionic mass transport into the PEDOT matrix during the redox process; Thirdly, direct interaction between the highly conjugated MWCNTs with high conductivity and the doped PEDOT effectively combine the double layer capacitance and Faradaic pseudocapacitance.

4. Conclusions

The MWCNTs@PEDOT/PSS core–shell composites have been prepared with a facile electrochemical polymerization method. This special core–shell nanostructure can significantly reduce the ions diffusion distance and the 3D porous nano-network microstructure effectively increases the specific surface area. The electrochemical characterizations indicate the incorporation of MWCNTs into the composites noticeably improve the capacitive performance compared to that of the pristine PEDOT electrodes. The MWCNTs@PEDOT/PSS composites exhibit a high areal capacitance of 98.1 mF cm^{-2} at 5 mV s^{-1} and retain the superb stability for 5000 CV cycles. This facile and effective approach for the electrodes preparation further extends the application of MWCNTs and can be easily transferred to flexible conductive substrate for future flexible electrochemical energy storage devices.

Acknowledgments

The authors appreciate funding from National Natural Science Foundation of China (21274082 and 21073115) and Shanxi Province (2012021021-3), the Program for New Century Excellent Talents in University (NCET-10-0926), and the Scientific Research Start-up Funds of Shanxi University (020351801002).

References

[1] S. Kondrat, P. Wu, R. Qiao, A.A. Kornyshev, Nat. Mater. 13 (2014) 387–393.
[2] M.F. El-Kady, V. Strong, S. Dubin, R.B. Kaner, Science 335 (2012) 1326–1330.
[3] H. Maruyama, H. Nakano, M. Nakamoto, A. Sekiguchi, Angew. Chem. Int. Ed. 53 (2014) 1324–1328.
[4] D. Guo, Y. Luo, X. Yu, Q. Li, T. Wang, Nano Energy 8 (2014) 174–182.
[5] R.Z. Ma, X.H. Liu, J.B. Liang, Y. Bando, T. Sasaki, Adv. Mater. 26 (2014) 4173–4178.
[6] L. Li, Z. Wu, S. Yuan, X.B. Zhang, Energ. Environ. Sci. 7 (2014) 2101–2122.
[7] Y.T. Weng, N.L. Wu, J. Power Sources 238 (2013) 69–73.
[8] Q. Lu, J.G.G. Chen, J.Q. Xiao, Angew. Chem. Int. Ed. 52 (2013) 1882–1889.
[9] D.H. Zhang, M.H. Miao, H.T. Niu, Z.X. Wei, ACS Nano 8 (2014) 4571–4579.
[10] L.J. Deng, J.F. Wang, G. Zhu, L.P. Kang, Z.P. Hao, Z.B. Lei, Z.P. Yang, Z.H. Liu, J. Power Sources 248 (2014) 407–415.
[11] Z.S. Wu, Y. Sun, Y.Z. Tan, S.B. Yang, X.L. Feng, K. Mullen, J. Am. Chem. Soc. 134 (2012) 19532–19535.
[12] Q. Chen, Y.N. Meng, C.G. Hu, Y. Zhao, H.B. Shao, N. Chen, L.T. Qu, J. Power Sources 247 (2014) 32–39.
[13] Y. Lin, X.Y. Wang, G. Qian, J.J. Watkins, Chem. Mater. 26 (2014) 2128–2137.
[14] A. Achour, J.B. Ducros, R.L. Porto, M. Boujtita, E. Gautron, L. Le Brizoual, M.A. Djouadi, T. Brousse, Nano Energy 7 (2014) 104–113.
[15] J.W. Lee, A.S. Hall, J.D. Kim, T.E. Mallouk, Chem. Mater. 24 (2012) 1158–1164.
[16] L. Huang, C. Li, G.Q. Shi, J. Mater. Chem. A 2 (2014) 968–974.
[17] Z.L. Wang, X.J. He, S.H. Ye, Y.X. Tong, G.R. Li, ACS Appl. Mater. Interfaces 6 (2014) 642–647.
[18] P. Simon, Y. Gogotsi, Nat. Mater. 7 (2008) 845–854.
[19] Y.P. Zhai, Y.Q. Dou, D.Y. Zhao, P.F. Fulvio, R.T. Mayes, S. Dai, Adv. Mater. 23 (2011) 4828–4850.
[20] S.L. Candelaria, Y. Shao, W. Zhou, X. Li, J. Xiao, J.-G. Zhang, Y. Wang, J. Liu, J. Li, G. Cao, Nano Energy 1 (2012) 195–220.
[21] S. Paul, K.S. Choi, D.J. Lee, P. Sudhagar, Y.S. Kang, Electrochim. Acta 78 (2012) 649–655.
[22] C. Oueiny, S. Berlioz, F.X. Perrin, Prog. Polym. Sci. 39 (2014) 707–748.
[23] H.Y. Mi, X.G. Zhang, S.Y. An, X.G. Ye, S.D. Yang, Electrochem. Commun. 9 (2007) 2859–2862.
[24] X.X. Bai, X.J. Hu, S.Y. Zhou, J. Yan, C.H. Sun, P. Chen, L.F. Li, Electrochim. Acta 87 (2013) 394–400.
[25] C. Peng, S.W. Zhang, D. Jewell, G.Z. Chen, Prog. Nat. Sci. 18 (2008) 777–788.
[26] J.P. Liu, J. Jiang, M. Bosman, H.J. Fan, J. Mater. Chem. 22 (2012) 2419–2426.
[27] Y.Y. Horng, Y.C. Lu, Y.K. Hsu, C.C. Chen, L.C. Chen, K.H. Chen, J. Power Sources 195 (2010) 4418–4422.
[28] A. Osterholm, T. Lindfors, J. Kauppila, P. Damlin, C. Kvarnstrom, Electrochim. Acta 83 (2012) 463–470.
[29] C.H. Lei, P. Wilson, C. Lekakou, J. Power Sources 196 (2011) 7823–7827.
[30] S. Bhandari, M. Deepa, A.K. Srivastava, A.G. Joshi, R. Kant, J. Phys. Chem. B 113 (2009) 9416–9428.
[31] Y.Q. Han, B. Ding, H. Tong, X.G. Zhang, J. Appl. Polym. Sci. 121 (2011) 892–898.
[32] H.J. Shin, S.S. Jeon, S.S. Im, Synth. Met. 161 (2011) 1284–1288.
[33] L. Chen, C.Z. Yuan, H. Dou, B. Gao, S.Y. Chen, X.G. Zhang, Electrochim. Acta 54 (2009) 2335–2341.
[34] D.X. Han, G.F. Yang, J.X. Song, L. Niu, A. Ivaska, J. Electroanal. Chem. 602 (2007) 24–28.
[35] D. Yu, K. Goh, H. Wang, L. Wei, W. Jiang, Q. Zhang, L. Dai, Y. Chen, Nat. Nanotechnol. 9 (2014) 555–562.
[36] K. V, E. Frackowiak, F. Beguin, Electrochim. Acta 50 (2005) 2499–2506.
[37] H.H. Zhou, G.Y. Han, Y.M. Xiao, Y.Z. Chang, H.J. Zhai, J. Power Sources 263 (2014) 259–267.
[38] H.G. Wei, J.H. Zhu, S.J. Wu, S.Y. Wei, Z.H. Guo, Polymer 54 (2013) 1820–1831.
[39] M.H. Yu, Y.X. Zeng, C. Zhang, X.H. Lu, C.H. Zeng, C.Z. Yao, Y.Y. Yang, Y.X. Tong, Nanoscale 5 (2013) 10806–10810.
[40] M. Jin, Y.Y. Liu, Y.L. Li, Y.Z. Chang, D.Y. Fu, H. Zhao, G.Y. Han, J. Appl. Polym. Sci. 122 (2011) 3415–3422.
[41] C. Peng, J. Jin, G.Z. Chen, Electrochim. Acta 53 (2007) 525–537.
[42] Y. Song, J.L. Xu, X.X. Liu, J. Power Sources 249 (2014) 48–58.
[43] N.J. Dudney, Electrochem. Soc. Interfaces 17 (2008) 44.
[44] H.L. Wang, C.M.B. Holt, Z. Li, X.H. Tan, B.S. Amirkhiz, Z.W. Xu, B.C. Olsen, T. Stephenson, D. Mitlin, Nano Res. 5 (2012) 605–617.
[45] Y.F. Xu, I. Hennig, D. Freyberg, A.J. Strudwick, M.G. Schwab, T. Weitz, K.C.P. Cha, J. Power Sources 248 (2014) 483–488.